JOURNAL OF CATALYSIS 40, 11–18 (1975)

Hydrogen–Water Deuterium Exchange over Nickel–Chromia Supported on Alumina[1]

II. Catalytic Activities and Effectiveness Factors

HONG-CHIU CHEN[2] AND NORMAN H. SAGERT

Research Chemistry Branch, Whiteshell Nuclear Research Establishment, Atomic Energy of Canada Limited, Pinawa, Manitoba, R0E 1L0, Canada

Received January 2, 1975

The activities of nickel and nickel–chromia on alumina catalysts for hydrogen–water deuterium exchange were measured with 5.5 mm diameter spheres in a fully mixed, fixed bed reactor and with powder of the same catalysts in a packed bed, flow reactor.

The promoting effect of chromia on the alumina supported nickel was not as large as it was for coprecipitated nickel–chromia catalysts. There was evidence that the alumina support was, itself, acting as a promotor. The activity was not affected by the nature of the anions in the impregnating solution used to prepare the catalyst, except for nickelous sulfate which gave much lower rates.

Powdered catalysts had a higher activity than large particles unless the nickel was in only the outer layers of the spheres. When the nickel was uniformly distributed throughout the spheres, the effectiveness factors could be calculated satisfactorily from the model of Wakao and Smith [*Ind. Eng. Chem. Fundam.* **3**, 123 (1964)]. This model was less satisfactory when the catalyst structure was altered by multiple impregnations followed by calcining. When the water pressure was much less than the hydrogen pressure, low effectiveness factors resulted largely from the slow diffusion of water in and out of the pores.

INTRODUCTION

Nickel–chromia catalysts have been found to be good catalysts for hydrogen–water deuterium exchange (*1,2*). These catalysts were coprecipitated from carbonates of nickel and chromium and contained about 85% nickel and 15% chromium. Catalysts were then prepared in a size and shape suitable for industrial use by pelletizing the precipitated carbonates (*1*). However, the preparation of catalysts by impregnation is potentially simpler, since the support can be obtained in various physical forms with different surface areas, pore volumes and pore diameters. Impregnation by different procedures can give different metal profiles and different catalyst physical properties.

In this work, the activities of several nickel–chromia catalysts supported on alumina were studied to provide criteria for the design of practical catalysts. The role of metal profiles and catalyst structure on the reaction kinetics has been assessed.

Hydrogen–water deuterium exchange has several advantages for these studies. The deuterium concentration can be kept low so that reaction (1) is the only reaction of importance.

$$H_2 + HDO \rightleftarrows HD + H_2O. \qquad (1)$$

Thus equilibrium is always approached by a first order process (*2,3*), and the kinetic analysis is simple. Heat effects are negligible, and the chemical composition remains constant in any type of reactor.

[1] AECL No. 5193.

[2] Present address: Chevron Research Co., Richmond, CA 94802.

Experimental effectiveness factors have been measured directly (*4*) under conditions where external mass transport was absent by measuring rates on large pellets and also on very small particles. Furthermore, by determining the pore structures of the catalysts, effectiveness factors can also be calculated and compared with the measured values. The morphology, total metal content, and metal distribution of the catalysts used have been described in a preceding article (*5*).

EXPERIMENTAL METHODS

Two reactors were used to measure the exchange rate. A small, packed bed reactor was used to measure exchange rates over crushed powder catalysts, and a stirred, fixed bed reactor was used for the catalyst pellets (*6*). The schematic arrangement of these reactors is shown in Fig. 1. Both reactors could be operated simultaneously and a valve allowed selection of the exit stream from either reactor for analysis.

The small reactor was identical to that described earlier (*7*). Since we wanted to determine intrinsic rates in this reactor, it was essential to show that both intraparticle and interparticle diffusion had been eliminated. These effects were examined by using catalyst powders of different mesh sizes, and by varying the quantities of catalyst at constant space velocity. Intraparticle diffusion effects would be revealed by different catalytic activities for different particle sizes, whereas interparticle diffusion effects would show as variations in the activities with flow rates at constant space velocity (*4*).

The stirred reactor was made from a 1-liter permanent magnet drive autoclave by attaching a four-vane catalyst basket to the stirrer shaft. The catalyst particles (0.5–2 g) were placed in the basket and rotated. To test the degree of mixing, glass beads were put into the basket to replace the catalyst and hydrogen was passed through the reactor. A pulse of argon (5 cm^3) was injected upstream from the reactor and the argon concentration in the hydrogen leaving the reactor was measured as a function of time (*6*). These mixing tests were carried out with various flow rates and stirring speeds.

For both reactors, ultra pure hydrogen (99.999%) was passed through a palladium-on-asbestos catalyst to remove any oxygen and was then saturated with water containing 3% D_2O by volume (6% HDO) in a saturator maintained at 63.3°C in a constant temperature bath. Corrections were made for the different volatilities of H_2O and HDO (*8*). The exchange reaction [reaction (1)] took place in the reactor and the effluent was passed through a condenser and a dry ice trap to remove the water. The hydrogen flow rates were measured with soap film flowmeters. The HD content of the hydrogen was measured mass spectrometrically (*9*). Flow rates were chosen so that the conversion did not exceed 60% of the equilibrium conversion. All measurements were made at a total pressure of about 100 kPa.

Prior to rate measurements, fresh cata-

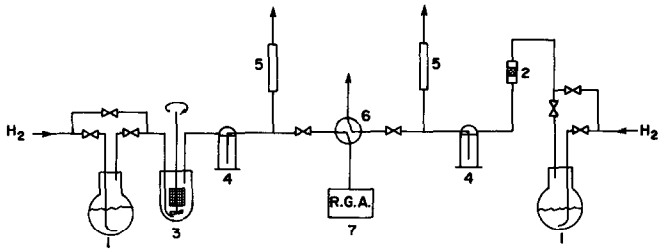

FIG. 1. Flow diagram of the reactor system: (1) heavy water saturator; (2) micro-packed-bed reactor; (3) stirred fixed-bed reactor; (4) dry ice trap; (5) soap film flowmeter; (6) four-way valve; (7) residual gas analyzer.

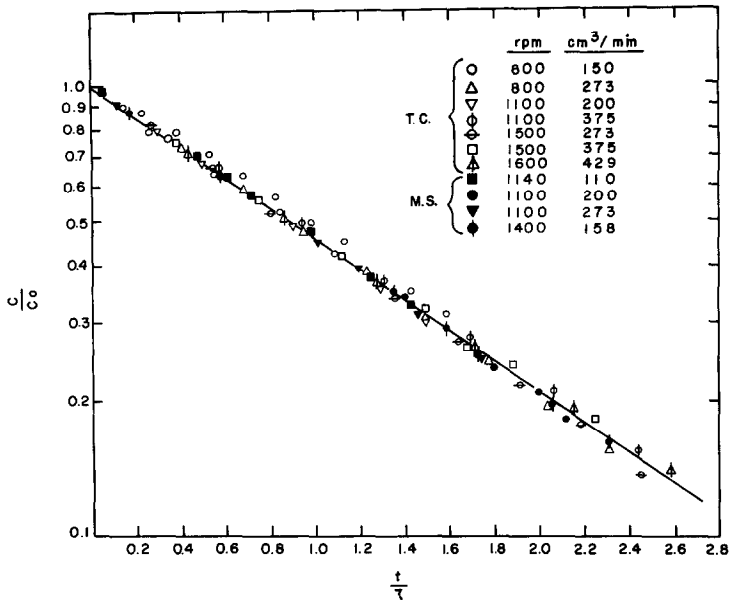

FIG. 2. Experimental results of mixing tests in the stirred flow reactor.

lysts were flushed with argon for at least 1 hr at 150°C and were then reduced in flowing hydrogen at 300°C for 16 hr, at a flow rate of at least 2 cm³(STP)/s.

RESULTS

The results of the argon mixing tests in the stirred reactor are shown in Fig. 2. Here t and τ are the elapsed time and space-time (the ratio of reactor volume to hydrogen volumetric flow rate), respectively. The argon concentration at $t = 0$ is given by C_0, and C is the concentration at time t. The straight line follows $(C/C_0) = \exp(-t/\tau)$ and represents instantaneous mixing in the reactor (*6*). At stirring rates greater than 800 rpm and flows greater than 110 cm³/min, complete mixing was achieved.

For reaction (1), the net rate of exchange, r, can be expressed as (*3,10*)

$$r = k_r[(1-n)N - n(1-N)/K], \quad (2)$$

where n is the mole fraction of HD in the hydrogen; N is the mole fraction of HDO in the water vapor; K is the equilibrium constant of reaction (1). The rate coefficient, k_r, would be the initial rate of reaction (1) in the forward direction for the exchange of deuterium between pure HDO and H_2 [Eq. (9)]. Of course, such experiments cannot be done since pure HDO would form an equilibrium mixture of H_2O, HDO, and D_2O. At low deuterium contents,

$$r \sim k_r(N - n/K). \quad (3)$$

The total deuterium content in any element of the reactor is conserved, so

$$F_{H_2}\, dn + F_{H_2O}\, dN = 0, \quad (4)$$

where F_{H_2} and F_{H_2O} are molar flow rates of hydrogen and water, respectively. This leads to

$$N = N_0 - \frac{n - n_0}{\pi}, \quad (5)$$

where the subscript 0 refers to the mole fractions of HD and HDO in the stream entering the reactor and π is P_{H_2O}/P_{H_2}. Thus

$$r = k_r\left[\left(N_0 + \frac{n_0}{\pi}\right) - n\left(\frac{1}{K} + \frac{1}{\pi}\right)\right]. \quad (6)$$

At equilibrium, denoted by the subscript e,

$$N_e = N_0 - \frac{n_e - n_0}{\pi} \tag{7}$$

and

$$K = \frac{n_e(1 - N_e)}{(1 - n_e)N_e} = \frac{n_e}{N_e}. \tag{8}$$

Thus

$$N_0 + \frac{n_0}{\pi} = n_e\left(\frac{1}{K} + \frac{1}{\pi}\right). \tag{9}$$

For the packed bed reactor

$$r = F_{H_2}\frac{dn}{dW_m} = k_r\left[\left(N_0 + \frac{n_0}{\pi}\right) - n\left(\frac{1}{K} + \frac{1}{\pi}\right)\right], \tag{10}$$

where W_m is the weight of nickel in the catalyst. Rearranging and integrating leads to (*3*)

$$k_r = \frac{1}{(1/K) + (1/\pi)}\left(\frac{F_{H_2}}{W_m}\right)\ln\frac{n_e - n_0}{n_e - n}. \tag{11}$$

For the fixed bed stirred reactor,

$$r = F_{H_2}\frac{(n - n_0)}{W_m} = k_r\left[\left(N_0 + \frac{n_0}{\pi}\right) - n\left(\frac{1}{K} + \frac{1}{\pi}\right)\right]. \tag{12}$$

This leads directly to an expression for k_r in the stirred reactor:

$$k_r = \left(\frac{1}{(1/K) + (1/\pi)}\right)\left(\frac{F_{H_2}}{W_m}\right)\left(\frac{n - n_0}{n_e - n}\right). \tag{13}$$

For the packed bed used with powdered catalysts, when $\ln[(n_e - n_0)/(n_e - n)]$ was plotted against $F^{-1}{}_{H_2}$ generally this plot was linear to fairly high conversions (*7*) and k_r was evaluated from the initial slope using Eq. (11). This procedure was necessary to eliminate the effects of back-diffusion (*9*). For the stirred reactor a true differential k_r could be calculated directly from Eq. (13). It should be emphasized again that k_r is the rate for reaction (1) in the forward direction.

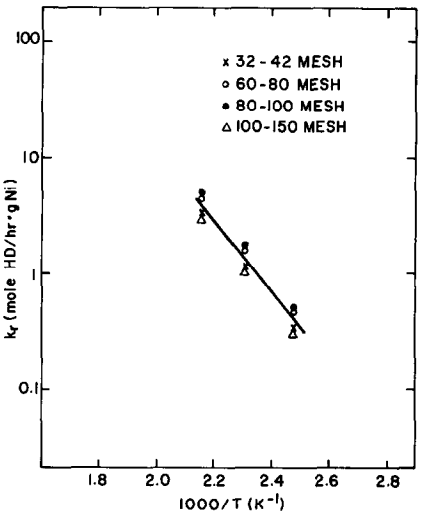

FIG. 3. Activity of catalyst 543 of different particle sizes in the flow reactor.

The activity of powdered catalyst 543 [see Ref. (*5*) for characterization] is shown in Fig. 3 for four mesh sizes. The activity varied somewhat at the three temperatures tested but since the variation was random with respect to particle size, it can be considered due to unknown experimental differences. Thus, intraparticle diffusional resistance was considered insignificant.

The same catalyst activities are shown in Fig. 4 plotted as a function of flow rate at constant space velocity. The activity of the catalysts remained essentially constant while the flow rate was varied by a factor of three. This leads to the conclusion that interparticle diffusional resistance is small.

Figure 5 shows the activity of catalyst 542 [Ref. (*5*), Table 1] both as the original spheres of 5.5 mm diameters, and as the crushed powder as a function of the temperature in an Arrhenius plot. Catalyst 542 was prepared by impregnation of the alumina support spheres with a solution containing 0.15 mol/liter of chromic nitrate and 0.71 mol/liter of nickelous nitrate. It had a reasonably flat nickel profile, although the nickel concentration was depleted in the region near the outside surface of the spheres and chromium was

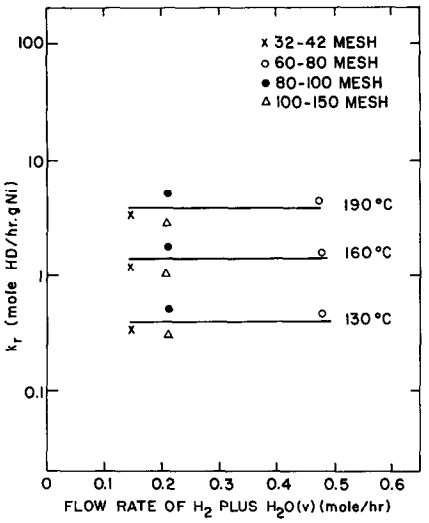

FIG. 4. Activity of catalyst 543 at different flow rates in the flow reactor.

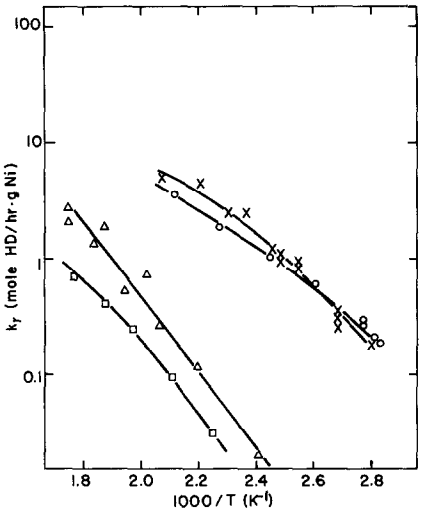

FIG. 6. The activity of catalysts 543 and 575 as spheres and as small particles: (×) 543 powder; (○) 543 spheres; (△) 575 powder; (□) 575 spheres.

concentrated in the outer region (*5*). Also shown are the activities of the spherical catalyst calculated from the rate over powders and efficiency factors which were computed from the catalyst pore structure as discussed below.

Figure 6 shows rate data from catalysts 543 and 575. Catalyst 543 was impregnated with 1.43 mol/liter nickelous nitrate, and had most of the nickel concentrated in the outer shell. Catalyst 575 was impregnated with 1.47 mol/liter nickelous sulfate to yield a fairly uniform concentration of nickel in the outer two thirds of the pellet and no nickel in the core (*5*). For catalyst 543, in fact, the spheres had about the same activity as the powder, indicating that the efficiency factor for the spheres was very high. Both catalysts 542 and 575 showed lower activities as spheres, indicating a lower efficiency factor for the spheres. As powder, catalyst 542 displayed a slightly higher activity per gram of nickel than catalyst 543. This indicated a slight promoting effect of chromia, but this promotion was much less effective than for the coprecipitated catalysts (*2*). Rates were very much lower for catalyst 575 which was prepared from nickelous sulfate solution. This was probably a result of the lower surface area (*5*) and the presence of sulfur in this catalyst.

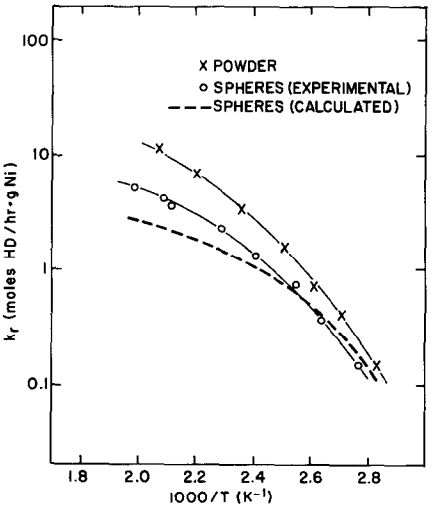

FIG. 5. The activity of catalyst 542 as 5.5 mm diameter spheres and as small particles. The origin of the calculated line is given in the text.

Figure 7 shows the activities of catalysts 578-U 578-V and 578-W as powder and of 578-U and 578-W in the form of spheres. Also shown are the calculated activities for catalyst 578-U and 578-W as spheres. These catalysts were prepared from nickelous nitrate and chromic acid solutions.

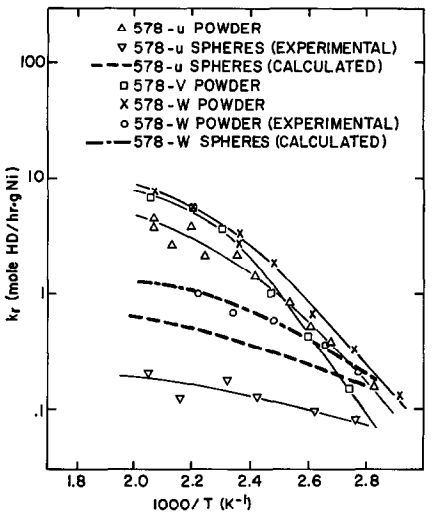

FIG. 7. The activity of catalysts 578-U, 578-V and 578-W as spheres and 578-U and 578-W as small particles. The origin of the calculated line for 578-U and 578-W as spheres is given in the text.

They were each prepared somewhat differently but all have similar concentration profiles (*5*). There was no significant variation in activity among them for the powdered catalysts. The activity of the spheres was much lower, indicating small efficiency factors.

DISCUSSION

Our measured rates, expressed as rates per unit weight of nickel, are three to four orders of magnitude higher when the nickel is supported on alumina than would be predicted from rates measured by other workers over bulk nickel (*2*). For example, at 130°C, the rate for catalyst 543 is about 0.4 mol HD/hr g Ni. At 79°C, the rate is 9×10^{-5} mol HD/hr g Ni for bulk nickel (*2*). Thus alumina seems to act as a promotor. Some of this promotion may be structural, but the bulk nickel used by Margineanu and Olariu (*2*) had a surface area of 4.4 m^2/g. Thus any increase in the nickel surface areas of our supported catalysts could not account for all the increase in rate. Therefore, a large proportion of the promotion by the support must be chemical. In fact, our measured rates were only slightly lower than rates measured over coprecipitated nickel–chromia catalysts containing the optimum amount of chromia (*2,10*). This also suggests that the alumina support is acting as a chemical promoter.

Recently it has been shown that alumina may act as a chemical promoter for nickel catalyzed hydrogen–water exchange (*11*). Thus the further effect of small additions of chromia is a factor of two at most (catalysts 543 and 542).

The very much lower activity of the catalyst prepared from nickelous sulfate is attributed to poisoning of the surface by sulfur. The surface area of this catalyst is also somewhat lower (132 m^2/g as against 163 m^2/g) suggesting that some of the pores may be plugged.

In all catalytic processes there are the physical and chemical steps of bulk phase mass transfer, pore diffusion, adsorption, surface reaction, desorption, pore diffusion and bulk phase mass transfer of products. Any of these processes can be rate limiting. We have attempted to eliminate bulk phase mass transfer by using the stirred reactor for large spheres, and appropriate flow conditions in the packed bed. Pore diffusion would be eliminated in the packed bed if our particles were small enough (*4*). The data in Fig. 3 suggest that this is the case. Thus, the rate data from the packed bed include the adsorption, reaction, and desorption terms which we shall call the intrinsic rate. The data obtained from the large spheres in the stirred bed should reflect pore diffusion and intrinsic rate. The ratio of the two gives the experimental effectiveness factor directly.

Ever since the concept of the effectiveness factor was introduced by Thiele (*12*), there has been much interest in evaluating effectiveness factors for reactions in porous material. Satterfield (*4*) has reviewed this work and has listed reactions for which the effectiveness factor has been determined by experiment, and where it has been compared to the theory. A number of theoretical treatments are pos-

sible, but for the catalysts considered here, which contain both macro- and micropores, the treatment developed by Mingle and Smith (*13*) and Wakao and Smith (*14*) seems especially apt. Their model has been well tested using ortho-para hydrogen conversion over NiO on alumina (*15,16*).

The model as developed by Wakao and Smith (*14*) treats first order reversible reactions in a solid consisting of small microporous particles forming a larger matrix with macropores between the small particles. For the small particles making up the pellet, the rate is expressed as (*16*)

$$r = k_w \eta_i (n_e - n). \qquad (14)$$

We will consider first the case where water diffusion is slow and assume hydrogen diffusion to be fast. We will return to this point later. In Eq. (14), η_i is the effectiveness factor of the small particles. Comparing Eqs. (14) and (3), it is apparent that k_r in Eq. (3) is the rate coefficient for reaction (1) in the forward direction only, whereas $k_w\ \eta_i$ in Eq. (14) is a rate constant for the first order equilibriation of reaction (1). Following the steps involved in deriving Eqs. (11) and (13), it can be shown that

$$k_w \eta_i = \frac{F_{H_2}}{W_m} \ln \frac{n_e' - n_0}{n_e' - n}, \qquad (15)$$

in the packed bed reactor, and

$$k_w \eta_i = \frac{F}{W_m} \frac{n_e' - n_0'}{n_e' - n'}, \qquad (16)$$

in the stirred reactor where the primes indicate conditions applying in the microporous particles. In other words, in the small particles

$$k_i \eta_i = k_r' \left(\frac{1}{K} + \frac{1}{\pi} \right). \qquad (17)$$

If the pellet effectiveness factor for the macropores is η_a, then for the spheres:

$$k_w \eta_i \eta_a = k_r \left(\frac{1}{K} + \frac{1}{\pi} \right). \qquad (18)$$

For an isotopic exchange reaction where the flux of each chemical species must be the same, the effective diffusivity, D, in the pellet is (*14*)

$$D = \frac{\epsilon_a^2}{(1/D_b) + (1/D_{ka})} + \frac{\epsilon_i^2 (1 + 3\epsilon_a)}{1 + \epsilon_a} \cdot \frac{\eta_i}{(1/D_b) + (1/D_{ki})} \qquad (19)$$

where the ϵ's are the void fractions and D's are diffusion coefficients. The subscript a refers to the macrovolume and the subscript i to the microvolume. The subscript b refers to a bulk diffusion coefficient and the subscript k to a Knudsen diffusion coefficient. These were calculated from an equation given by Satterfield (*4*), employing the pore radii previously measured (*5*). Since the elementary particles of the sphere are of the order of a few tens of micrometers, and since we have already shown that there is no noticeable effect of pore diffusion for particles as large as 400 μm (40 mesh), η_i was taken as 1.0. With D evaluated, η_a could be calculated (*13*) using Eq. (20)

$$\eta_a = 3 \frac{h_s \coth h_s - 1}{h_s^2}; \qquad h_s = R_0 \left(\frac{\eta_i k_w R T}{D P_{H_2O}} \rho_B \right)^{1/2}, \qquad (20)$$

where ρ_B is the bulk density and R_0 is the radius of the sphere. Effectiveness factors so calculated and applied to the rates measured over crushed catalyst in the packed bed reactor gave the calculated rates over the large sphere. These calculated rates are shown in Figs. 5 and 7.

Up to this point we have considered the case where water diffusion was responsible for any diffusional limitations in the catalyst, and hydrogen gradients were small. When we considered the case where water was in equilibrium and the diffusion of hydrogen was rate controlling, η_a was always greater than 0.85 and was generally greater than 0.95. The high effectiveness factors, compared to those calculated for water seemed to result from the higher

hydrogen pressure used [see Eq. (20)]. Therefore water diffusion in and out of the pores appears to be the primary cause of small effectiveness factors.

For catalyst 542, the model predicts the effectiveness factors well at lower temperatures but predicts lower rates than were actually observed at higher temperatures (Fig. 5). This catalyst is deficient in nickel at the outer edges, but has chromia in the outer edges. At higher temperatures, relatively more of the reaction takes place in the outer region where the promoting effect of chromia is measurable. Also, the pore structure used in the model was that for alumina impregnated with nickel. This is probably not applicable in the outer region. Catalyst 543 has most of its nickel in the outer shell and consequently has an effectiveness factor of 1.0 over the entire range of temperature.

For catalyst 578-W, the model predicts the measured rates extremely well, whereas the measured rates over catalyst 578-U were much lower than predicted. These catalysts had essentially similar metal distributions with nickel spread uniformly throughout the sphere and a small quantity of chromia at the edges. Catalyst 578-U was made by impregnation with a single solution containing both chromium and nickel, whereas catalyst 578-W was impregnated with chromium, dried, calcined, and impregnated with nickel. The latter technique clearly gave a less active catalyst. Since the rates over crushed powder are not greatly different, the rate differences for the spheres must be physical in nature rather than chemical. It would seem that prior calcining with chromic acid present resulted in a finer macropore structure which hinders diffusion.

In summary, the addition of chromia as a promoter for nickel catalyzed hydrogen–water deuterium exchange is much less effective for alumina supported nickel than for coprecipitated nickel–chromia catalysts because the alumina itself seems to act as a chemical and structural promoter. For catalysts made by impregnation with a single solution, the pore diffusion model of Wakao and Smith (*14*), using catalyst parameters obtained from nickel impregnated catalysts, predicts the efficiency factors observed. Prior impregnation followed by calcining appears to alter the pore structure so as to vary as a function of depth in the sphere. This invalidates the model and makes the predictions inaccurate.

ACKNOWLEDGMENT

The authors are grateful to the National Research Council of Canada for providing Postdoctoral Fellowships to H.C.C.

REFERENCES

1. Taylor, E. H., "Production of Heavy Water" (G. M. Murphy, H. C. Urey, and I. Kirshenbaum, Eds.), McGraw-Hill, New York, 1955.
2. Margineanu, P., and Olariu, A., *J. Catal.* **8,** 359 (1967).
3. Rolston, J. H., and Goodale, J. W., *Can. J. Chem.* **50,** 1900 (1972).
4. Satterfield, C. N., "Mass Transfer in Heterogeneous Catalysis" MIT Press, Cambridge, MA, 1970.
5. Chen, H. C., Sagert, N. H., and Jones, S., *J. Catal.* **39,** 1–10 (1975).
6. Tajbl, D. G., Simons, J. B., and Carberry, J. J., *Ind. Eng. Chem. Fundam.* **5,** 171 (1966).
7. Sagert, N. H., and Pouteau, R. M. L., *Can. J. Chem.* **49,** 3411 (1971).
8. Kirshenbaum, I., *in* "Physical Properties and Analysis of Heavy Water (H. C. Urey and G. M. Murphy, Eds.). McGraw-Hill, New York, 1951.
9. Sagert, N. H., and Pouteau, R. M. L., *Can. J. Chem.* **51,** 4031 (1973).
10. Fodor, T., Margineanu, P., and Olariu, A., *Stud. Cercet. Fiz.* **22,** 697 (1970).
11. Abou El-nour, F., and Schuetze, H., *Isotopenpraxis* **8,** 391 (1972).
12. Thiele, E. W., *Ind. Eng. Chem.* **31,** 916 (1939).
13. Mingle, J. O., and Smith, J. M., *AIChE J.* **7,** 243 (1961).
14. Wakao, N., and Smith, J. M., *Ind. Eng. Chem. Fundam.* **3,** 123 (1964).
15. Rao, M. R., and Smith, J. M., *AIChE J.* **9,** 485 (1963).
16. Rao, M. R., Wakao, N., and Smith, J. M., *Ind. Eng. Chem. Fundam.* **3,** 127 (1964).